ISSN 0023-1584, Kinetics and Catalysis, 2022, Vol. 63, No. 1, pp. 97–107. © The Author(s), 2022. This article is an open access publication.
Russian Text © The Author(s), 2022, published in Kinetika i Kataliz, 2022, Vol. 63, No. 1, pp. 110–121.

This manuscript is dedicated to the memory of Roman Alekseevich Buyanov, our teacher and mentor, an outstanding Russian scientist, a true son of his Fatherland

Carbon Erosion of a Bulk Nickel–Copper Alloy as an Effective Tool to Synthesize Carbon Nanofibers from Hydrocarbons

I. V. Mishakov[a, b, *], S. D. Afonnikova[a, b], Yu. I. Bauman[a], Yu. V. Shubin[b, c], M. V. Trenikhin[d], A. N. Serkova[a], and A. A. Vedyagin[a]

[a] *Boreskov Institute of Catalysis, Russian Academy of Sciences, Novosibirsk, 630090 Russia*
[b] *Novosibirsk State University, Novosibirsk, 630090 Russia*
[c] *Nikolaev Institute of Inorganic Chemistry, Siberian Branch, Russian Academy of Sciences, Novosibirsk, 630090 Russia*
[d] *Center of New Chemical Technologies, Boreskov Institute of Catalysis, Russian Academy of Sciences, Omsk, 644040 Russia*
**e-mail: mishakov@catalysis.ru*

Received September 9, 2021; revised September 20, 2021; accepted September 20, 2021

Abstract—Carbon erosion of bulk metals and alloys in a carbon-containing atmosphere can be used as an effective tool for the targeted synthesis of carbon nanomaterials. In this study, a set of bulk $Ni_{0.89}Cu_{0.11}$ (11 at % Cu) alloys has been synthesized by the mechanochemical alloying of metal powders in an Activator 2S planetary mill. The synthesized samples have been studied as precursors of catalyst for the synthesis of carbon nanofibers (CNFs) from ethylene at 550°C. The effect of the activation time on the particle morphology and phase composition of the alloys, the kinetics of growth, and the carbon product yield in C_2H_4 decomposition has been studied. For the most active samples, the CNF yield has exceeded 100 g/g_{cat} within 30 min of reaction. The early stage of carbon erosion of a bulk $Ni_{0.89}Cu_{0.11}$ alloy has been studied by electron microscopy methods. It has been found that the nucleation of carbon fiber growth active sites occurs during a short-term contact of the sample with the reaction mixture (less than 1 min); the complete disintegration of the alloy is observed in a few minutes. The carbon product is represented by nanofibers having a submicrometer diameter and characterized by a dense "stacked" and coaxial-conical packing of graphene layers. The material has a developed specific surface area (140–170 m^2/g) and a low bulk density (less than 30 g/L).

Keywords: nickel, copper, bulk alloys, mechanochemical alloying, ethylene, carbon erosion, carbon nanofibers

DOI: 10.1134/S0023158422010049

INTRODUCTION

Scientists all over the world has long recognized carbon nanomaterials (CNMs) as one of the most science-intensive and promising directions in the development of nanotechnology [1]. The development of methods for the controlled synthesis of CNMs, along with the improvement of the catalysts used, is an important present-day problem being solved at the intersection of knowledge of catalysis and materials science. A significant contribution to the development of fundamental concepts and practical advances in this direction has been made by Corresponding Member of the Russian Academy of Sciences Roman Alekseevich Buyanov, who has proposed a carbide cycle mechanism (CCM) to describe the formation of carbon nanostructures over metal catalysts [2–4]. A distinctive feature of the activities conducted at Boreskov Institute of Catalysis under the supervision of R.A. Buyanov was their focus on studying the mechanism of the catalytic synthesis of carbon materials and methods for controlling these processes [5]. The latest studies of Roman Alekseevich were aimed at diligently developing the concept of the so-called "physicochemical nanorobot" (PCNR), in which the nanorobot is considered as a multifunctional catalytic nickel particle, which is simultaneously responsible for the decomposition of a carbon-containing substrate and

Abbreviations and notation: CNMs, carbon nanomaterials; CCM, carbide cycle mechanism; PCNR, physicochemical nanorobot; CE, carbon erosion; CNTs, carbon nanotubes; CNFs, carbon nanofibers; MCA, mechanochemical alloying; XRD, X-ray diffraction analysis; CSR, coherent scattering region; SEM, scanning electron microscopy; TEM, transmission electron microscopy; IP, induction period.

the atomic–molecular "assembly" of carbon nanostructures [6–8]. Advances in the further development of science in this field can be associated with the search for new methods of "programming" these nanorobots to provide the formation of carbon nanostructures with a desired set of characteristics.

Nickel-based catalysts should apparently be attributed to the most widespread systems used in actual practice to synthesize CNMs of various types [9, 10]. In turn, nickel–copper alloys hold a unique position among Ni–M bimetallic alloy catalysts, because they are the most active, stable, and affordable [11–13]. The methods used to synthesize nickel–copper catalysts are multivarious; in many cases, they reduce to the preparation of nanosized particles of a Ni–Cu alloy and their stabilization on the surface of various supports (SiO_2, Al_2O_3, MgO, etc.) [14–16]. The typical disadvantages of supported catalysts include the sintering of metal nanoparticles during a reduction treatment at high temperatures, the limited yield of the carbon product due to the rapid deactivation of particles of a nonoptimum size, and the difficulty of removing the impurity of a mineral component (support) from the composition of the produced carbon material.

Is there a method to synthesize a catalyst in which all active particles "by origin" have a required composition and an optimum size that determines the maximum efficiency of the catalyst under particular reaction conditions? Here, it is pertinent to mention the carbon erosion (CE) of bulk metals and alloys, which is known for the ability to slowly destroy the material of the walls of industrial reactors made of steel or nickel alloys [17–19]. The problem is associated with the fact that, at a temperature of 400–800°C, iron and nickel are capable of dissolving carbon [20], which subsequently precipitates in the form of a graphite-like phase in the region of interblock boundaries and leads to the degradation of the polycrystalline structure of the product [21]. The disintegration of a bulk alloy leads to the transformation of the system into a different quality determined by the appearance of a large number of dispersed particles (alloy fragments) that catalyze the growth of fibrous carbon [22–24]. It is generally accepted that CE (referred to as metal dusting in the foreign literature) is an extremely slow process characterized by a long induction period (IP) lasting a few hundred hours [21, 25]. At the same time, in the case of using coke-generating hydrocarbons (such as butadiene [24, 26] or ethylene [27, 28]) and corrosive chlorine-substituted hydrocarbons [29, 30], the complete degradation of the bulk alloy can occur within several hours and even minutes. In this case, a bulk alloy (for example, Ni–M) can be considered as a precursor of a catalyst resulting from the spontaneous disintegration of the alloy under reaction conditions [31].

It should be noted that recently CE has been increasingly used for the targeted synthesis of various CNMs (in particular, carbon nanotubes (CNTs) and nanofibers (CNFs)) and hybrid metal–carbon composites and catalysts [27, 32, 33]. It has been found that this approach is particularly effective in the case of the catalytic decomposition of chlorine-substituted hydrocarbons (1,2-dichloroethane, trichlorethylene, etc.) and waste based on them to produce CNFs [29, 34]. It has been shown that the rapid disintegration of microdispersed Ni–M alloys leads to the formation of active particles with a similar size, in the presence of which chlorohydrocarbons are subsequently converted to carbon filaments with a unique segmented structure [35, 36]. It has been found that this "self-organizing catalyst" formed under the action of a carbon-containing reaction medium is extremely stable and efficient compared with conventional supported systems [31].

In this manuscript, an example of the use (as a catalyst precursor) of bulk Ni–Cu (11 at % Cu) alloys synthesized by the mechanochemical alloying (MCA) of individual metal powders in a planetary mill is discussed. Ethylene is selected as the reactive hydrocarbon. The effect of the activation time of the composites on their morphological features and catalytic activity in CNF synthesis is studied. The early stage of the CE of Ni–Cu alloys, which is characterized by the nucleation and formation of active particles that catalyze the growth of carbon filaments, is studied in detail.

EXPERIMENTAL

Starting Reagents

Bulk Ni–Cu alloys were synthesized using the PNK-UT3 nickel powder (State Standard GOST 9722-97, NPO Rusredmet) and the PMS-1 copper powder (GOST 4960-2009, OOO Spetspostavka). Catalytic tests were conducted using ethylene (high purity grade, GOST 24975.1, Nizhnekamskneftekhim) and high purity grade argon and hydrogen.

Synthesis and Characteristics of Catalyst Precursors

A set of Ni–Cu alloys (catalyst precursors) was prepared by MCA using an Activator 2S planetary mill (OOO Aktivator, Russia). Before the synthesis, a premix was prepared by mixing nickel and copper powders in a weight ratio of Ni/Cu = 88/12. After that, a weighed portion of the premix in an amount of 10 g was loaded into a steel drum (V = 250 mL) together with grinding balls made of stainless steel (340 g). The diameter of the grinding bodies was 5 mm. The grinding body-to-premix weight ratio was 340/10 = 34 g/g in all experiments.

The rotation frequency of the drums and the platform was controlled using a VF-S15 industrial frequency inverter (Toshiba, Indonesia). The rotation

frequency of the drums and the central axis was 449 and 956 rpm, respectively. The calculated acceleration of the grinding bodies was 784 m/s^2 (~80 g). During activation, the drums were water cooled to avoid overheating. The activation (alloying) time of the composite was varied in a range of 3–11 min. During the experiment, the drums were periodically stopped after 3, 5, 7, and 9 min to take samples in an amount of ~100 mg and then study their morphology and phase composition. Upon the completion of the MCA procedure, the drums were unloaded in air; the resulting samples of Ni–Cu alloys were separated from the grinding bodies using a sieve and weighed.

For convenience, the set of alloy samples was designated as follows: NiCu_x/y, where $x = D_{gb}$ (diameter of grinding bodies), $y = \tau$ (activation time).

Carbon Product Accumulation Kinetics Investigation Procedure

The kinetics of carbon product accumulation on the catalyst was studied in a real time mode using a gravimetric flow unit equipped with a McBain balance. A weighed portion of a bulk alloy sample in an amount of 1.50 ± 0.02 mg was placed in a foamed quartz bowl, suspended using a quartz spring, and loaded into a quartz flow reactor. After that, the sample was heated in an argon stream to the reaction temperature (550°C). The heating rate was 10°C/min. Upon achieving a given temperature, the sample was brought into contact with a reaction mixture of the following composition: ethylene (18 vol %), hydrogen (59 vol %), and argon (the rest). The total feed rate of the reaction mixture was 66 L/h. The change in the sample weight due to the deposition of the carbon product was recorded every 2 min using a cathetometer. The catalytic test time was 30 min. Upon the completion of the test, the reactor was cooled to room temperature in an argon stream. The resulting carbon material sample was unloaded and weighed; next, the specific yield of CNFs in grams per gram of catalyst (g/g_{cat}) was calculated. In addition, bulk density (g/L) was measured for all CNF samples.

Physicochemical Investigation Procedures for the Samples

X-ray diffraction (XRD) analysis was conducted on a Shimadzu XRD-7000 diffractometer (Shimadzu, Japan) using CuK_α radiation (Ni filter) at a wavelength of 1.54178 Å. To determine the phase composition, scanning was performed in a 2θ angle range of 20°–100° in increments of 0.05°. Phases were identified using the PDF database [37]. For a more accurate calculation of cell parameters, scanning was performed in an angular range of 2θ = 140°–147° in increments of 0.05° and an acquisition time of 10 s per point. The crystal cell parameters of solid solutions were determined from the position of the 331 reflection using the PowderCell 2.4 software [38]. Average crystallite size (coherent scattering region (CSR)) was calculated from the broadening of the 111, 200, and 220 reflections using the Scherrer equation [39]. The calculation of the CSR and the description of diffraction reflections by the Pearson function were conducted using the WinFit 1.2.1 software [40]. Crystallographic parameters for pure metals (Ni and Cu) were taken from the JCPDS-PDF database [41].

The secondary structure of the bulk alloys and the morphology of the carbon product were studied by scanning electron microscopy (SEM) on a JSM-6460 electron microscope (JEOL, Japan) at a magnification of 1000–100000×. The primary structure of the carbon product was studied by transmission electron microscopy (TEM) using a JEM 2100 microscope (JEOL, Japan; accelerating voltage, 200 kV; resolution, 0.14 nm).

The textural characteristics of the synthesized CNM samples were determined by low-temperature nitrogen adsorption/desorption. Adsorption isotherms were measured at 77 K on an ASAP-2400 automated instrument (Micromeritics, United States). The predegassing of the CNF samples was conducted at a temperature of 250°C for 6 h.

RESULTS AND DISCUSSION

Investigation of the Morphology and Phase Composition of Bulk Alloy Samples

At the first stage of the study, the effect of the activation time of the Ni + Cu mixture in a planetary mill on the secondary structure, morphology, and phase composition of the resulting samples was studied. Figure 1 shows SEM micrographs of the initial mixture of nickel and copper powders (premix, images 1a–1c) and the alloy samples that were activated for 5 min (images 1d–1f) and 11 min (images 1g–1i) under identical conditions. It is evident that the morphology of the powder particles in the composition of the sample undergoes significant changes during the mechanical impact. The secondary structure of the initial premix is represented by irregularly shaped agglomerates consisting of a large number of primary particles sintered to each other, the size of which does not exceed 2–3 μm (Fig. 1c). The agglomerate size varies over an extremely wide range, as evident from the survey image (Fig. 1a).

Figures 1d–1f show that a 5-min MCA procedure leads to dramatic changes in the morphology of the powder particles. The activation leads to the flattening of the particles to form characteristic plates with a thickness of a few micrometers. The surface of these plates can be assumed conventionally smooth, with the presence of characteristic sagging resulting from the plastic deformation of the metal (Fig. 1f) [42–44]. Comparison of images in Figs. 1a and 1d shows that, during the mechanical impact, the powder particles

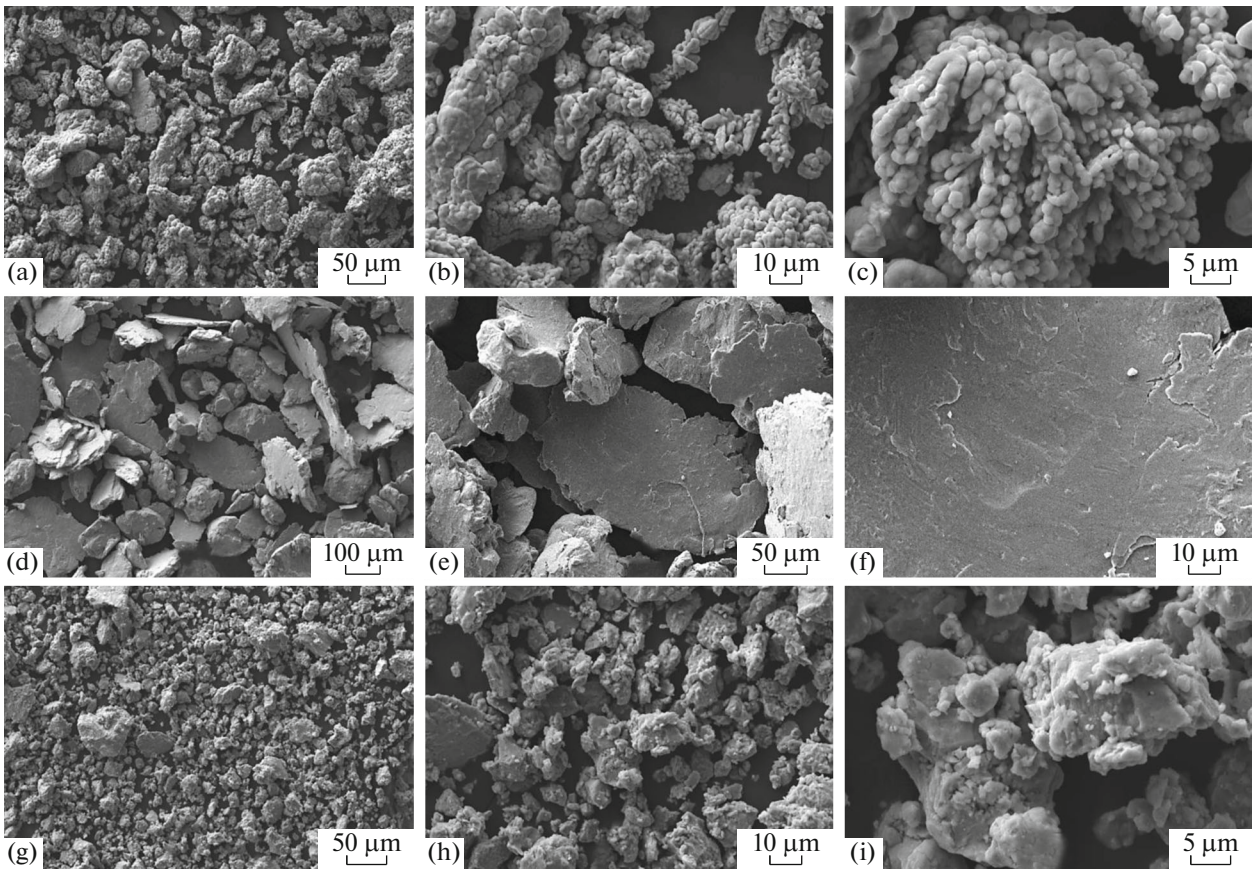

Fig. 1. Evolution of the morphology of particles of the Ni–Cu alloy sample during MCA: (a–c) 0 min (initial premix), (d–f) 5 min (sample NiCu_5/5), and (g–i) 11 min (sample NiCu_5/11) according to SEM.

significantly coarsen compared with the particles of the initial premix. An increase in the activation time of the sample to 11 min also causes fairly significant changes in the morphology, namely, the complete disappearance of the plate-like shape of the particles and a pronounced decrease in the average agglomerate size. A large number of extremely small crystallites are observed on the surface of the secondary particles; this fact apparently indicates the secondary agglomeration of the particles (Fig. 1i) [42]. Note that the observed tendencies in the change in the size and morphology of the particles of the activated bimetallic composite are in good agreement with the published data [43, 44]. During the activation of a composite consisting of a mixture of ductile metals, upon collision with grinding bodies, the particles initially are flattened to form a layered structure (plates) and then undergo degradation to form a fine powder [44].

Figure 2 and Table 1 show XRD analysis results for a set of Ni–Cu samples differing in the duration of the MCA procedure (3, 7, and 11 min of activation).

Comparison of the diffraction patterns of the premix (Fig. 2a, curve *1*) and the NiCu_5/3 sample (Fig. 2a, curve *2*) shows the presence of individual phases of nickel and copper in the two samples. This is evidenced by the invariable cell parameter of nickel (a = 3.524(1) Å, Table 1) and the presence of characteristic "shoulders" in the region of 2θ ~ 43° and 50° corresponding to the Cu impurity phase (face-centered cubic (fcc)). This result indicates the absence of an interaction phase: a Ni–Cu solid solution is not formed. However, the 3-min activation leads to a significant broadening of the diffraction peaks, which is particularly pronounced in the far-angle region (Fig. 2b, curve *2*). In this case, the CSR size decreases almost threefold (from 52 to 18 nm, Table 1).

With an increase in the activation time to 7–11 min, the picture changes qualitatively: a Ni–Cu solid solution based on the fcc lattice of nickel is formed. This conclusion is supported by the disappearance of reflections corresponding to the copper phase and the characteristic shift of the X-ray peaks toward small angles. This shift can be most clearly observed in the region of the 331 reflection (2θ ~ 145°, Fig. 2b, curves *3, 4*). In this case, the lattice cell parameter increases from 3.525 to 3.531–3.534 Å (Table 1). It should also be noted that the average crystallite size (CSR) gradually decreases with an increase in the activation time (to 8–10 nm, Table 1). According to the literature, there are no thermodynamic

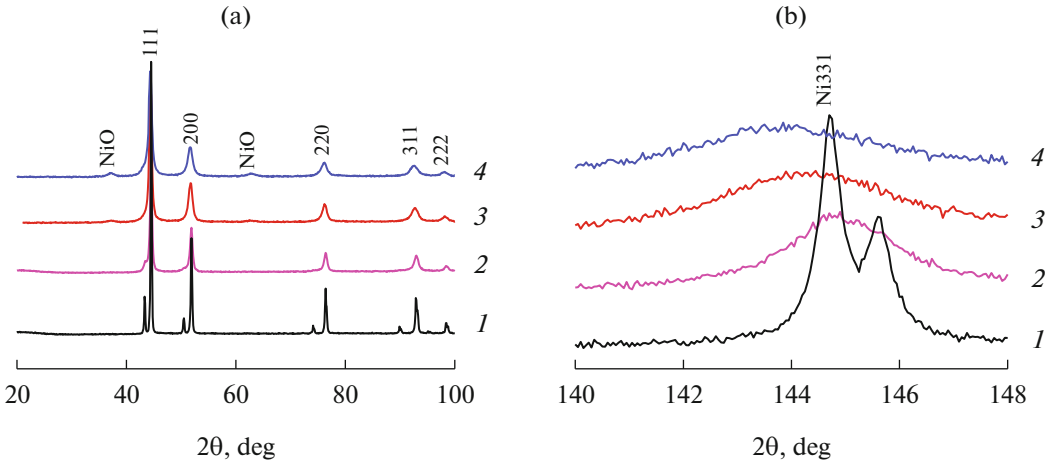

Fig. 2. Diffraction patterns in 2θ regions of (a) 20°–100° and (b) ~145° (reflection 331) for Ni–Cu samples prepared by the MCA method at the different activation durations τ: (*1*) 0 (premix), (*2*) 3, (*3*) 7, and (*4*) 11 min.

restrictions to the solubility of copper in nickel, because the Ni–Cu system is characterized by a continuous series of solutions [45].

It is evident from diffraction patterns *3* and *4* (Fig. 2a) that the formation of the Ni–Cu alloy is also accompanied by the appearance of additional reflections in the region of 2θ ~ 38° and 62°. These peaks are assigned to the nickel oxide (NiO) phase. The formation of a nickel oxide impurity in the samples can be attributed to the partial oxidation of the activated surface of the alloy, which occurs due to oxygen chemisorption upon a contact of the freshly prepared sample with air.

Thus, the MCA of metal powders in a planetary mill makes it possible to synthesize a bulk nickel–copper alloy (nickel-based Ni–Cu solid solution) within a relatively short time (τ > 3 min). This method is a single-stage waste-free procedure, which does not involve a high-temperature treatment. The prepared samples of bulk Ni–Cu alloys were subsequently tested as catalyst precursors in ethylene decomposition to form CNFs.

Catalytic Decomposition of Ethylene in the Presence of Bulk Ni–Cu Alloys

At the next stage, the kinetics of ethylene decomposition to form CNFs in the presence of the synthesized alloys was studied. It should be emphasized once again that these samples are catalyst precursors, because intense CE leads to their disintegration to form a large number of dispersed particles that catalyze the further CNF growth in accordance with the CCM [46].

Table 1. X-ray characteristics of the synthesized samples according to XRD analysis

Sample	Synthesis conditions			Cell parameter, Å	CSR, nm	Phase composition
	D_{gb}, mm	τ, min	additional conditions of treatment			
Premix	–	–	–	3.525	52	Mixture of Ni and Cu phases
NiCu_5/3	5	3	–	3.524	18	Mixture of Ni and Cu phases
NiCu_5/7	5	7	–	3.531	10	Ni–Cu solid solution NiO traces
NiCu_5/11	5	11	–	3.534	8	Ni–Cu solid solution NiO traces
*CNF_NiCu_5/7_550C_1'	5	7	t_r = 1 min; T = 550°C	3.532	26	Graphite Ni–Cu solid solution

D_{gb} is the diameter of grinding bodies (steel balls); t_r is the contact time between the sample and the reaction mixture at 550°C.
* The carbon gain in the sample was 99% (in terms of the weight of the alloy sample).
Dashes indicate that information is not available.

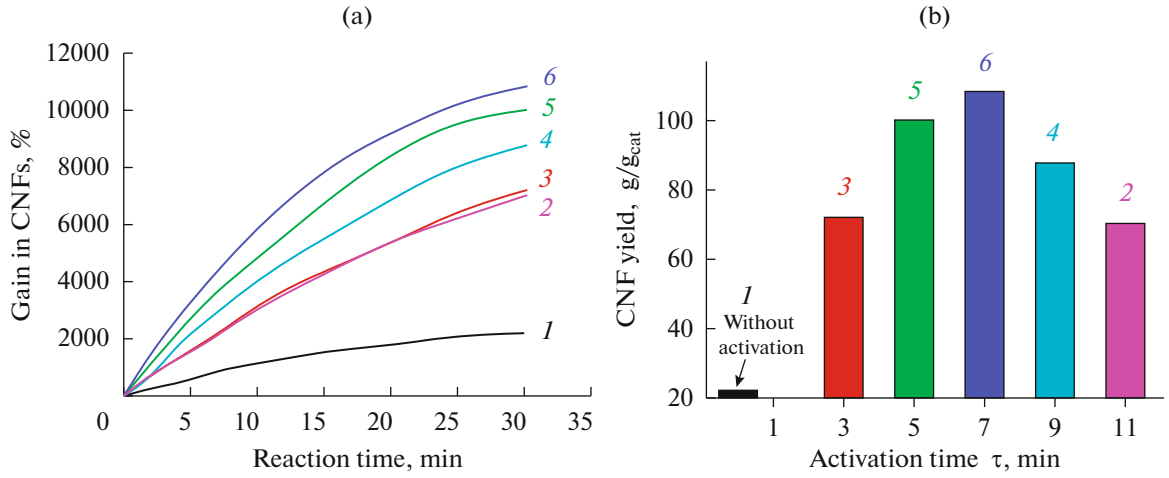

Fig. 3. Effect of the activation time (τ) of the Ni–Cu alloy on (a) the kinetics of accumulation of the carbon product and (b) the specific CNF yield within 30 min of the reaction: (*1*) premix; τ = (*2*) 11, (*3*) 3, (*4*) 9, (*5*) 5, and (*6*) 7 min. Reaction conditions: $C_2H_4/H_2/Ar$, $T = 550°C$.

Figure 2a shows kinetic curves for the carbon product accumulation on the catalyst, which were recorded in the real time mode. For all the samples, the time of interaction with the reaction mixture was 30 min. A premix sample that was not subjected to MCA was tested for comparison (Fig. 3a, curve *1*).

The results show that the alloying time has a decisive effect on the catalytic properties of the Ni–Cu sample. Thus, without activation, the productivity of the sample (premix) is minimal: it rapidly deactivates, as evidenced by the rapid appearance of a plateau in the kinetic curve (Fig. 3a, curve *1*); the achieved CNF yield does not exceed 25 g/g$_{cat}$ (Fig. 3b, Table 2). The result is attributed to the fact that copper does not have a stabilizing effect on the catalytic activity of nickel, because the metals in the premix do not interact [47].

At the same time, it is evident that the use even of a short-term activation (3 min) provides an abrupt increase in the growth rate of the carbon product over the alloy (Fig. 3a, curve *3*), which leads to an increase in the specific yield of CNFs to 72.1 g/g$_{cat}$ (Table 2). This significant increase in catalytic activity can apparently be associated with a closer interaction between nickel and copper, which contributes to the easy formation of the alloy in a reducing atmosphere at the reaction temperature.

With an increase in the activation time of the alloy to 7 min (sample NiCu_5/7), the highest growth rate of CNFs is achieved (Table 2); the productivity of the NiCu_5/7 catalyst is 108.4 g/g$_{cat}$ within 30 min of the reaction. A further increase in the alloying time leads to an abrupt decrease in the activity of the alloy. It is noteworthy that, for the NiCu_5/3 and NiCu_5/11 samples (τ = 3 and 11 min), the kinetic curves almost coincide (Fig. 3a, curves *2, 3*); in the presence of these samples, the CNF yield is approximately 1.5 times lower than the maximum value (Table 2). The observed dome-shaped dependence (Fig. 2b) indicates the existence of an optimum MCA time. An insufficient time of activation of the composite (as well as excessive) negatively affects the catalytic properties of the resulting nickel–copper alloy sample. Thus, it can be concluded that there are boundaries of opti-

Table 2. Effect of the activation time of the Ni + Cu composite on the CNF growth rate and the specific CNF yield in ethylene decomposition at 550°C and a reaction time of 30 min

Sample	Activation time (τ), min	Specific accumulation rate of CNFs*, %/min	Weight gain of the weighed portion, %	Yield of CNFs, g/g$_{cat}$
CNF_Premix	0	70	2200	22.0
CNF_NiCu_5/3	3	260	7210	72.1
CNF_NiCu_5/5	5	380	10020	100.2
CNF_NiCu_5/7	7	400	10840	108.4
CNF_NiCu_5/9	9	290	8780	87.8
CNF_NiCu_5/11	11	240	7030	70.3

* Calculated from kinetic curves in a reaction time range of 5–20 min.

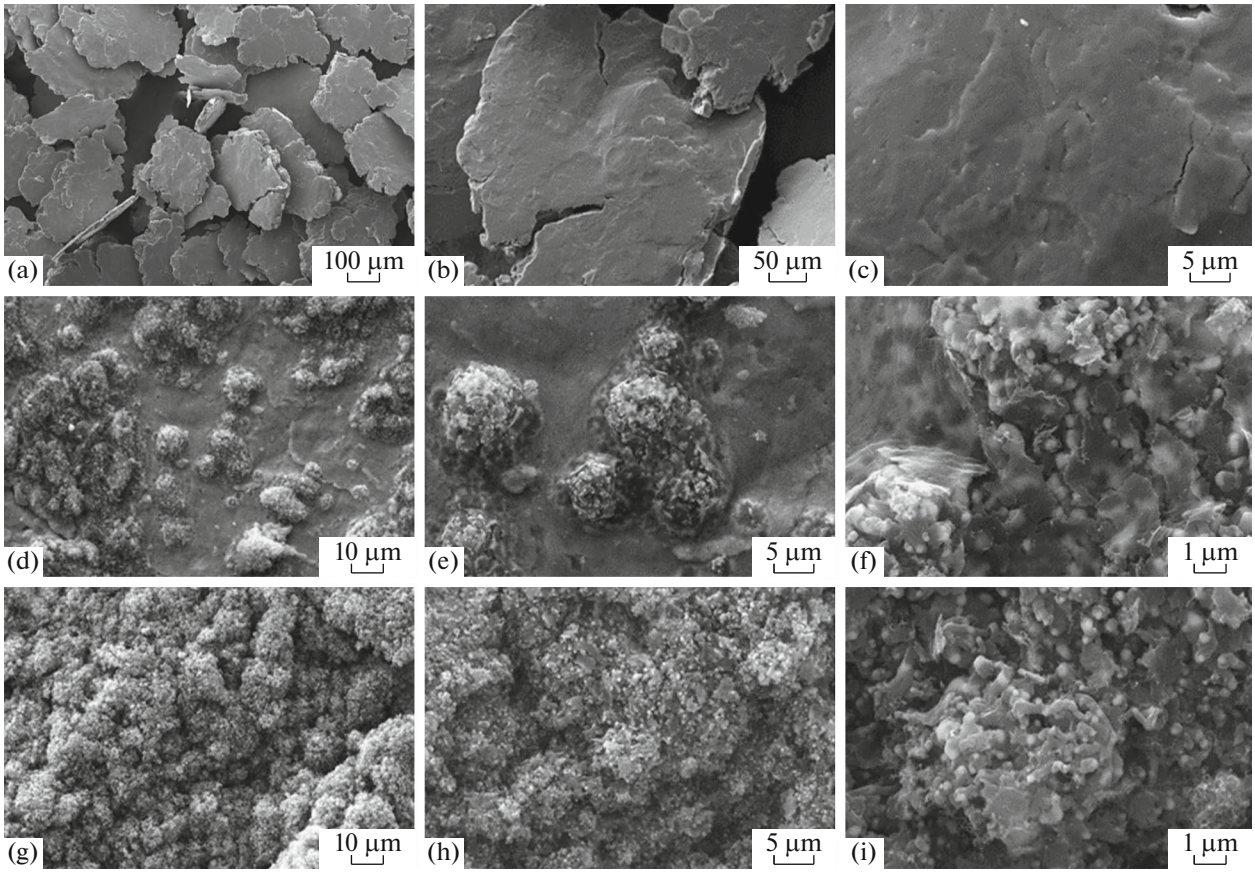

Fig. 4. Effect of a short-term exposure to a C_2H_4/H_2/Ar reaction mixture at 550°C on the secondary structure of the NiCu_5/7 sample (D_{gb} = 5 mm, τ = 7 min): (a–c) 0 min (initial alloy), (d–f) 30 s, and (g–i) 1 min according to SEM.

mum values within which the parameters of the MCA of metals should be varied to achieve the most efficient productivity of the alloy catalyst.

To summarize this section, it should be noted that the kinetic curves of CNF growth over bulk Ni–Cu alloys have the following important feature (Fig. 3a): almost complete absence of an IP phase. At the same time, upon a contact of bulk nickel-based alloys with other reaction gases (CO + H_2 [23, 25], CO + CO_2 [48], $C_2H_4Cl_2$ + H_2 [29, 30]), the IP time can be up to a few tens or even hundred hours. The presence of an IP phase is attributed to the slow occurrence of the CE process, which leads to the disintegration of the bulk alloy and the subsequent growth of carbon nanostructures [31]. In the case of interaction of a C_2H_4/H_2 mixture with Ni–Cu samples, the intensive growth of CNFs begins almost immediately, without an apparent "delay"; this fact indicates an extremely rapid degradation of the bulk alloy under the action of CE.

The next section will be focused on a detailed study of the processes that occur at the early stage of interaction of bulk Ni–Cu alloys with the reaction medium.

Investigation of the Early Stage of CE of Ni–Cu Alloys

Figure 4 shows SEM micrographs for NiCu_5/7, which is the most active sample, before and after contact with the reaction gas. As noted above, the initial alloy sample is represented by a set of large flakes with a conventionally smooth surface, which has traces of the shear action of steel grinding bodies moving at an acceleration of about 80 g (Figs. 4a–4c).

Next, the processes that occur on the surface of this alloy after an extremely short-term interaction with the reaction mixture (0.5–1 min) will be discussed in detail. The images in Figs. 4d–4f show the result of a 30-s exposure of a bulk alloy to a carbon-containing atmosphere at T = 550°C at the different magnifications. It is evident that the conventionally smooth surface of the bulk alloy breaks and becomes looser (Fig. 4f). An increase in the contact time to 1 min leads to the topography loosening over the entire surface of the alloy sample (Figs. 4g–4i).

Based on the XRD analysis data, it can be argued the observed changes are attributed to the appearance of a graphite-like phase (Fig. 5a, diffraction pattern *2*). In this case, all reflections corresponding to the Ni–Cu solid solution phase are preserved, while the inten-

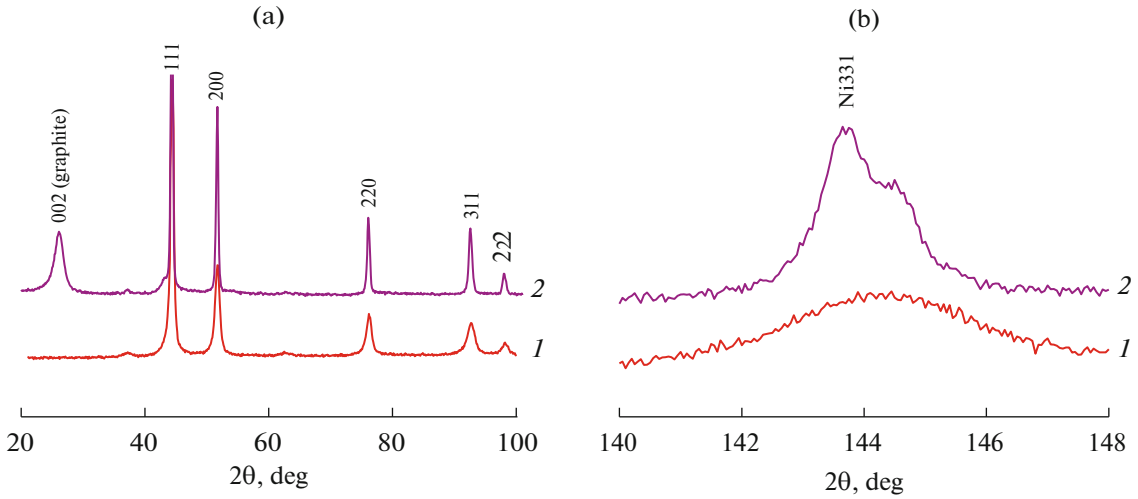

Fig. 5. Diffraction patterns of (*1*) the NiCu_5/7 alloy and (*2*) the CNF_NiCu_5/7_550C_1' sample formed due to a short-term contact of the NiCu_5/7 alloy with the reaction mixture (C_2H_4/H_2/Ar, T = 550°C, 1 min): the 2θ region of (a) 20°–100° and (b) ~145° (reflection 331).

sity of the peaks of the NiO impurity abruptly decreases. In the far angle region (Fig. 5b, diffraction pattern *2*), a change in the shape of the peak due to the annealing of defects and an increase in the degree of crystallinity of the alloy are observed. In this case, the CSR size also increases from 8 to 26 nm (Table 1). It should also be noted that the 331 reflection is further shifted to the region of small angles (Fig. 5b, diffraction pattern *2*) compared with that of the initial sample; this shift can be attributed to the appearance of nonstoichiometric carbides (interstitial solutions) due to the incorporation of carbon atoms into the alloy lattice at the early stage of CE. The formation of these carbides was observed earlier in studying the decomposition of 1,2-dichloroethane in the presence of $Ni_{1-x}Pd_x$ and $Ni_{1-x}Pt_x$ alloys [36, 49].

Let us return to the SEM images in Fig. 4. Upon closer examination (Figs. 4f, 4i), the contours of already formed active particles of a submicrometer size (0.1–0.3 μm) can be observed; subsequently, these particles act as active sites catalyzing ethylene decomposition and the growth of carbon filaments. Figure 6 shows a set of SEM and TEM images, in which the morphology of active particles formed due to the disintegration of the alloy is quite clearly visible. The SEM images recorded in the back-scattered electron mode (Figs. 6a, 6b) clearly show an array of formed dispersed crystals (white contrasting spots) that emerged on the sample surface. Figure 6c shows a TEM image, in which dispersed active particles formed due to the fragmentation of the bulk alloy are clearly visible. Note that each dispersed particle of the alloy is bound with at least two short carbon filaments (Figs. 6b–6d).

The TEM micrographs in Figs. 6d and 6e show active particles having different morphologies. The first particle has a symmetric biconical shape (Fig. 6d); it is "responsible" for the formation of carbon filaments with a coaxial-conical packing of graphene layers [50]. The second particle (Fig. 6e) is visually bound with three filaments, in the structure of which the basal planes of graphite are packed parallel to the deposition face, which corresponds to the so-called "stacked" structure of CNFs [46].

Thus, as a consequence of the rapidly occurring CE process, in just 1 min, the initially coarse alloy (particle size of up to 100 μm and more) is transformed into an active catalyst represented by a set of dispersed alloy particles that mediate the CNF growth in accordance with the CCM. Owing to the spontaneous nucleation of active CNF growth particles due to disintegration, these systems can be referred to as a self-organizing catalyst [35, 36]. Some other authors believe that the fragmentation of bulk alloys based on iron and nickel occurs due to the deposition of the graphite phase in the region of grain boundaries of the polycrystalline structure of the alloy [21, 51]. During the degradation of the alloy structure under the action of CE, dispersed particles with a submicrometer diameter, the size of which is suitable for the implementation of the CCM, are spontaneously formed. Even at the very beginning of CNF growth, a differentiation of the functions of the different crystal faces is observed. According to the terminology proposed by R.A. Buyanov, the first type of faces is responsible for the decomposition of hydrocarbon molecules ("frontal" faces), and the other type ("rear" faces) is responsible for the graphite deposition process and the CNF growth [3, 46].

Recall that the weight gain of the carbon product for the CNF_NiCu_5/7_550C_1' sample is about 100%, which is also evident from the results of kinetic

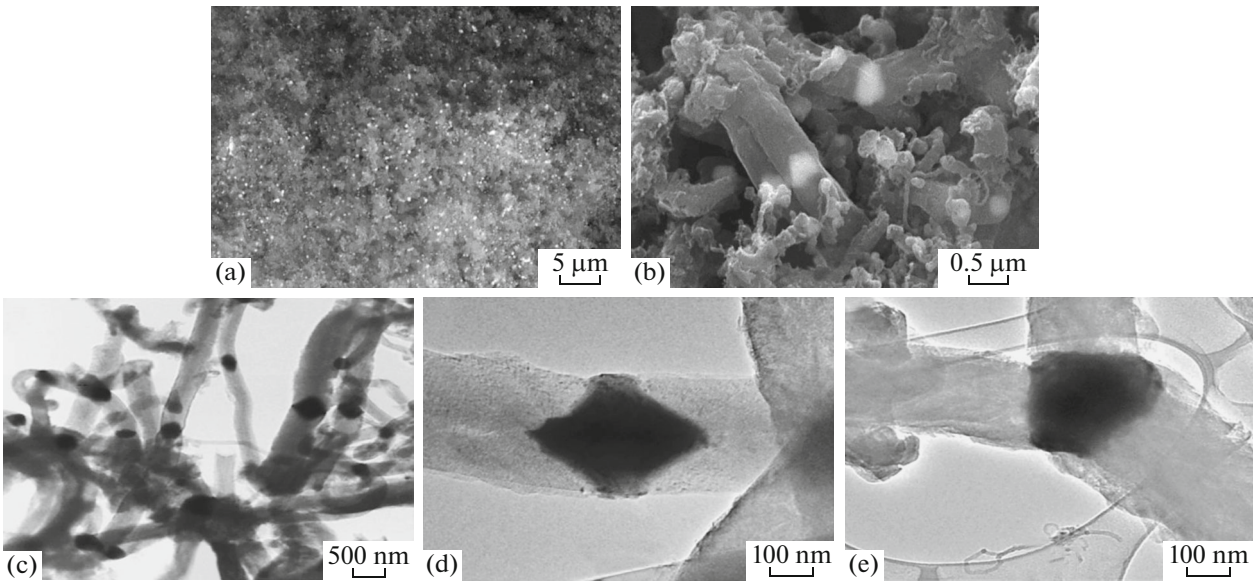

Fig. 6. Morphology of active particles formed due to a 1-min contact of the NiCu_5/5 alloy sample (D_{gb} = 5 mm, τ = 5 min) with the reaction gas: (a, b) SEM images in the back-scattered electron mode and (c–e) TEM images.

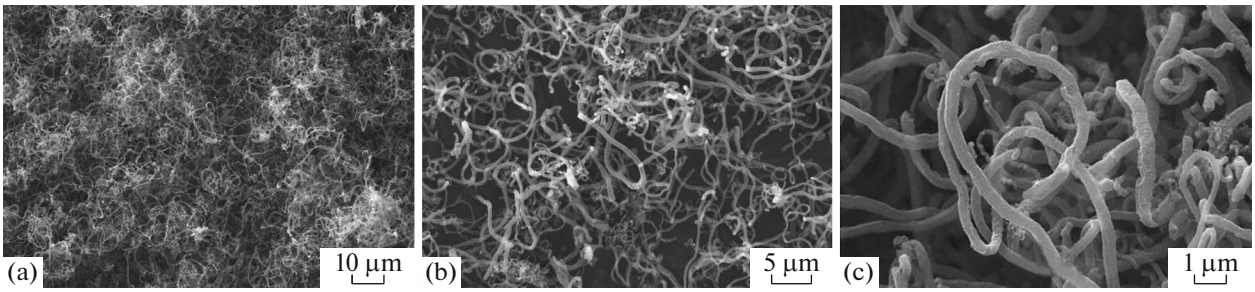

Fig. 7. Scanning electron microscopy images of CNFs synthesized due to the 30-min interaction of ethylene with the NiCu_5/5 sample at 550°C. The CNF yield is 108.4 g/g_{cat}.

measurements (Fig. 3a). It can be assumed that, with a twofold increase in the sample weight, the initial bulk alloy undergoes almost complete disintegration to form active particles, which are CNF growth sites. Let us try to determine the approximate number of active particles formed from an alloy with a weight of 1 g. Assuming that the average active particle size is 250 nm, it is possible to calculate the theoretical number of CNF growth sites formed due to the complete disintegration of 1 g of the initial Ni–Cu alloy. According to our estimates, it is about 1.4×10^{13} pieces per gram of precursor.

The further growth of carbon filaments catalyzed by active particles of the nickel–copper alloy occurs in accordance with the CCM. Figure 7 shows SEM images of the carbon product. It is evident that the CNM formed due to a 30-min interaction of bulk Ni–M alloys with ethylene is represented by a set of long carbon filaments with a submicrometer diameter (Fig. 7c). As noted above, the filaments are characterized by a fairly dense packing of graphene layers to form a structure of two types—stacked and coaxial-conical.

According to low-temperature nitrogen adsorption (Brunauer–Emmett–Teller method), the synthesized CNM is characterized by a developed specific surface area (140–170 m^2/g) and a fairly low porosity (0.14–0.22 cm^3/g). It should be noted that this material exhibits unusual macroscopic properties. Despite the high specific yield of CNFs (more than 100 g/g_{cat}), the synthesized carbon product has an extremely low bulk density (no more than 30 g/L). Apparently, this loose packing of carbon filaments partially entangled with each other arises as early as the time when the bulk alloy undergoes disintegration, during which bundles of parallel growing nanofibers are formed (Figs. 6b, 6c). The parallel growth of carbon fibers is a characteristic feature of self-organizing catalysts operating on the principle of CE of bulk metals and alloys [31].

CONCLUSIONS

In this study, an example of using bulk nickel–copper alloys for the targeted synthesis of CNFs from ethylene has been discussed. Mechanochemical alloying of metals has been selected as the method for synthesizing bulk Ni–Cu alloys, because it is the most simple, convenient, and efficient technique, which makes it possible to avoid the "wet chemistry" and high-temperature calcination stages. The MCA method provides the researcher with a set of parameters (activation time, diameter of grinding bodies, the ratio of rotation speeds of drums and platforms, etc.) that can be varied to synthesize alloy composites with optimum properties. In this study, the effect of the activation time on the morphology, phase composition, and catalytic properties of Ni–Cu alloys has been studied, and an optimum mode providing a high carbon product yield (more than 100 g/g_{cat} within 30 min of reaction) has been found.

The evolution of the structure and composition of the bulk Ni–Cu alloy at the early stage of CE has been studied in detail. It has been shown that the CE of the alloy is a rapid process, as evidenced by the almost complete absence of an IP phase in the kinetic curve of CNF growth. The disintegration of the bulk Ni–Cu alloy leads to the formation of a catalyst system consisting of a large number of active submicrometer particles separated by growing carbon filaments. Let us emphasize that, in this approach to synthesizing the catalyst, the necessary stage of the active component predispersion is as if omitted to let the reaction system choose the optimum size of active particles "by itself." It is these active particles formed from a bulk precursor under reaction conditions that have every chance to prove themselves as a stable and effective CNM synthesis catalyst. In addition, note that the composition of the synthesized carbon product is completely free of impurities of hard-to-remove mineral components (for example, oxide supports).

The further functioning of catalytic growth sites formed due to CE occurs in accordance with the thoroughly studied CCM. According to the concept of a PCNR proposed by R.A. Buyanov, a polycrystalline particle of a nickel alloy can be considered as a nanorobot combining several different physicochemical functions ranging from the dissociation of hydrocarbon molecules to the atomic–molecular assembly of carbon nanostructures [6–8]. In the case under discussion, the product of this "assembly" is CNFs with a coaxial-conical and stacked structure.

To summarize, let us quote Roman Alekseevich Buyanov; in the series of his latest papers on the concept of a PCNR, he wrote, "Nature—in its infinite diversity—creates functional structures that govern nanotechnology. At the same time, it strives to find the simplest solutions in its creations. It is this that gives rise to the saying, "The genius lies in the simplicity of the solution."

FUNDING

This work was supported by the Ministry of Science and Higher Education of the Russian Federation within the framework of a state task to Boreskov Institute of Catalysis of the Siberian Branch of the Russian Academy of Sciences (project no. AAAA-A21-121011390054-1). The alloy samples were synthesized within the framework of a project of the Russian Foundation for Basic Research (project no. 18-29-19053-mk).

ACKNOWLEDGMENTS

The authors thank A.B. Ayupov for his assistance in the texture analysis of the CNF samples. The physicochemical properties of the samples were analyzed using the equipment of the Center for collective use "National Center for Research of Catalysts" and the Omsk Regional Center for collective use of the Siberian Branch of the Russian Academy of Sciences.

CONFLICT OF INTEREST

The authors declare that they have no conflicts of interest.

REFERENCES

1. Begum, S., Karim, A.N.M., Ansari, M.N.M., and Hashmi, M.S.J., *Encyclopedia of Renewable and Sustainable Materials*, 2020, p. 515.
2. Zaikovskii, V.I., Chesnokov, V.V., and Buyanov, R.A., *Kinet. Catal.,* 2006, vol. 47, no. 4, p. 603.
3. Buyanov, R.A. and Chesnokov, V.V., *Katal. Prom-sti,* 2006, no. 2, p. 3.
4. Buyanov, R.A., *Kinet. Katal.,* 1980, vol. 21, no. 1, p. 237.
5. Buyanov, R.A. and Mishakov, I.V., *Chem. Sustainable Dev.*, 2019, vol. 27, no. 2, p. 167.
6. Buyanov, R.A. and Parmon, V.N., *Khim. Interesah Ustoich. Razvit.*, 2016, vol. 24, no. 5, p. 705.
7. Buyanov, R.A. and Parmon, V.N., *Nanotech. Russ.*, 2015, vol. 10, nos. 3–4, p. 205.

8. Buyanov, R.A. and Parmon, V.N., *Katal. Prom-sti*, 2013, no. 3, p. 199.
9. Aboul-Enein, A.A., Soliman, F.S., and Betiha, M.A., *Int. J. Hydrogen Energy*, 2019, vol. 44, no. 59, p. 31104.
10. Shen, Y., Ge, M., and Lua, A.C., *Catal. Sci. Technol.*, 2018, vol. 8, no. 15, p. 3853.
11. Karimi, S., Bibaka, F., Meshkania, F., Rastegarpanahb, A., Dengb, J., Liub, Y., and Daib, H., *Int. J. Hydrogen Energy*, 2021, vol. 46, p. 20435.
12. Pod"yacheva, O.Yu., Shmakov, A.N., Ismagilov, Z.R., and Parmon, V.N., *Dokl. Phys. Chem.*, 2011, vol. 439, no. 1, p. 127.
13. Efremov, V.N. and Golosman, E.Z., *Kinet. Catal.,* 2006, vol. 47, no. 5, p. 782.
14. Torres, D., Pinilla, J.L., and Suelves, I., *Catalysts*, 2018, vol. 8, no. 8, p. 300.
15. Gutta, N., Velisoju, V.K., Tardio, J., Patel, J., Satyanarayana, L., Sarma, A.V., and Akula, V., *Energy Fuels*, 2019, vol. 33, no. 12, p. 12656.
16. Awadallah, A.E., *Chem. Pap.*, 2015, vol. 69, no. 2, p. 316.
17. Palsson, N.S., Kaewkumsai, S., Wongpinkaew, K., and Khonraeng, W., *J. Failure Anal.*, 2017, vol. 17, no. 5, p. 838.
18. Al-Meshari, A., van Zyl, G., and Al-Musharraf, M., *J. Failure Analysis Prev.*, 2017, vol. 17, no. 3, p. 363.
19. Taghipour, M., Eslami, A., Bahrami, A., and Ghalambaz, M., *Eng. Failure Analysis.*, 2020, vol. 115, p. 104656.
20. Buyanov, R.A., *Khim. Interesah Ustoich. Razvit.*, 2000, vol. 8, no. 3, p. 347.
21. Zhang, J. and Young, D.J., *Corros. Sci.*, 2007, p. 1496.
22. Chun, C.M., Bhargava, G., and Ramanarayanan, T.A., *J. Electrochem. Soc.*, 2007, p. 231.
23. Wu, Q., Zhang, J., and Young, D.J., *Mater. Corros.*, 2011, vol. 62, no. 6, p. 521.
24. Buyanov, R.A., Mishakov, I.V., and Vedyagin, A.A., *Dokl. Phys. Chem.*, 2013, vol. 448, no. 3, p. 11.
25. Ghorbani, H., Rashidi, A.M., Rastegari, S., Mirdamadi, S., and Alaei, M., *Mater. Res. Bull.*, 2011, vol. 46, p. 716.
26. Buyanov, R.A., Chesnokov, V.V., and Afanas'ev, A.D., *Kinet. Katal.,* 1979, vol. 20, no. 1, p. 207.
27. Yan, X.-L., Wu, Y.-L., Wang, B.-S., Zhang, Q., Zheng, R.-T., Wu, X.-L., and Cheng, G.-A., *Appl. Surf. Sci.*, 2018, p. 38.
28. Thakur, D.B., Tiggelaar, R.M., Gardeniers, J.G., Lefferts, L., and Seshan, K., *Surf. Coat. Technol.*, 2009, vol. 203, no. 22, p. 3435.
29. Bauman, Yu.I., Mishakov, I.V., Buyanov, R.A., Vedyagin, A.A., and Volodin, A.M., *Kinet. Catal.,* 2011, vol. 52, no. 4, p. 547.
30. Bauman, Yu.I., Kenzhin, R.M., Volodin, A.M., Mishakov, I.V., and Vedyagin, A.A., *Chem. Sustainable Dev.*, 2012, no. 20, p. 119.
31. Mishakov, I.V., Vedyagin, A.A., Bauman, Y.I., Shubin, Y.V., and Buyanov, R.A., *Carbon Nanofibers: Synthesis, Applications and Performance*, Nova Science, 2018, p. 77.
32. Camilli, L., Scarselli, M., Gobbo, S.D., Castrucci, P., Nanni, F., Gautron, E., Lefrant, S., and Crescenzi, M.D., *Carbon*, 2011, p. 3307.
33. Varanasi, C.V., Bulmer, J., Brunke, L., Burke, J., Baca, J., Yost, K., and Barnes, P., *J. Vac. Sci. Technol., A*, 2008, vol. 26, no. 4, p. 832.
34. Bauman, Yu.I., Mishakov, I.V., Vedyagin, A.A., Dmitriev, S.V., Mel'gunov, M.S., and Buyanov, R.A., *Katal. Prom-sti.,* 2012, no. 2, p. 261.
35. Bauman, Y.I., Shorstkaya, Y.V., Mishakov, I.V., Plyusnin, P.E., Shubin, Y.V., Korneev, D.V., Stoyanovskii, V.O., and Vedyagin, A.A., *Catal. Today,* 2017, vols. 293–294, p. 23.
36. Bauman, Y.I., Mishakov, I.V., Popov, A.A., Rieder, D., Korneev, D.V., Serkova, A.N., Shubin, Y.V., and Vedyagin, A.A., *Catal. Today,* 2020, vol. 348, p. 102.
37. *Powder Diffraction File. PDF_2/Release* 2009*: International Centre for Diffraction Data*, USA.
38. Nolze, G. and Kraus, W., *Powder Diffr.*, 1998, vol. 13, p. 256.
39. Cullity, B.D., *Elements of X-Ray Diffraction*, Massachusetts: Addison–Wesley, 1978, 2nd ed.
40. Krumm, S., *Mater. Sci. Forum*, 1996, vols. 228–231, no. 1, p. 183.
41. *JCPDS – PDF Database – International Centre for Diffraction Data, PCPDFWIN v. 2.02*, 1999.
42. Boldyrev, V.V., *Russ. Chem. Rev.*, 2006, vol. 75, no. 3, p. 177.
43. Suryanarayana, C., *Prog. Mater. Sci.*, 2001, vol. 46, nos. 1–2, p. 1.
44. Charlot, F., Gaffet, E., Zeghmati, B., Bernard, F., and Niepce, J.C., *Mater. Sci. Eng.,* 1999, vol. A 262, p. 279.
45. Hansen, M. and Anderko, K., *Constitution of Binary Alloys*, New York: McGraw-Hill, 1958.
46. Chesnokov, V.V. and Buyanov, R.A., *Russ. Chem. Rev.*, 2000, vol. 69, no. 7, p. 623.
47. Fenelonov, V.B., Derevyankin, A.Yu., Okkel, L.G., Avdeeva, L.B., Zaikovskii, V.I., Moroz, E.M., Salanov, A.N., Rudina, N.A., Likholobov, V.A., and Shaikhutdinov, Sh.K., *Carbon*, 1997, vol. 35, no. 8, p. 1129.
48. Chang, J.-K., Tsai, H.-Y., Lin, K.-Y., Tsai, W.-T., Wang, C.-Y., and Yu, M.-S., *ECS Transact.*, 2008, vol. 6, no. 17, p. 45.
49. Bauman, Y.I., Mishakov, I.V., Rudneva, Y.V., Plyusnin, P.E., Shubin, Y.V., Korneev, D.V., and Vedyagin, A.A., *Ind. Eng. Chem. Res.*, 2019, p. 685.
50. Zaikovskii, V.I., Chesnokov, V.V., Buyanov, R.A., and Plyasova, L.M., *Kinet. Catal.,* 2000, vol. 41, no. 4, p. 538.
51. Schmid, B., Aas, N., Grong, Ø., and Ødegård, R., *Appl. Catal., A*, 2001, p. 257.

Translated by M. Timoshinina